Conference Paper, Published Version

Rocca, Michele La; Prestininzi, Pietro; Mele, Paolo; Hinkelmann, R.

A Gas-Kinetic Model for Shallow Water Flows in Presence of Wet/Dry Fronts

ICHE 2014, Hamburg - Lehfeldt & Kopmann (eds) - © 2014 Bundesanstalt für Wasserbau ISBN 978-3-939230-32-8

A Gas-Kinetic Model for Shallow Water Flows in Presence of Wet/Dry Fronts

M. La Rocca, P. Prestininzi & P. Mele
Dipartimento di Ingegneria, Università degli Studi Roma Tre, Rome, Italy

R. Hinkelmann
Fachgebiet Wasserwirtschaft und Hydrosystemmodellierung, Institut für Bauingenieurwesen, Technische Universität Berlin, Berlin, Germany

ABSTRACT: Recently the single relaxation time Lattice Boltzmann Method (hereinafter LBM) has considerably spread in Computational Hydraulics. Such a diffusion is motivated by the fact that the corresponding numerical algorithm is much simpler than the ones derived from "classical" hydraulic models, such as e.g. the Shallow Water (hereinafter SW) equations. The main drawback of the standard LBM-based model of the SW equations is that it cannot simulate transcritical and supercritical SW flows, which very often occur in realistic situations. Such a serious shortcoming depends on the low number of lattice velocities usually adopted in standard LBM-based models of SW equations. If the number of lattice velocity is arbitrarily increased (i.e. an infinite number of lattice velocity is adopted), numerical simulations of transcritical and supercritical SW flows are possible. This is the basic idea of the Gas Kinetic Method (hereinafter GKM), recently extended to the simulation of SW flows. The aim of this work is to assess the ability of the finite volume formulation of the GKM recently proposed in literature when simulating SW flows in presence of wet/dry fronts and transcritical flows. The assessment is performed through a comparison with a considerable number of benchmark cases, both theoretical and experimental, 1D and 2D. Results are promising.

Keywords: Lattice Boltzmann Method, Gas Kinetic Method, Shallow Water Flows

1 INTRODUCTION

In the last two decades the single relaxation time Lattice Boltzmann Method (hereinafter LBM) spread considerably in Computational Hydraulics (Succi, 2001; Zhou; 2004, Aidun and Clausen, 2010). The main reason for such a development is that the corresponding numerical algorithm is much simpler than the usual numerical algorithms adopted for the Shallow Water (hereinafter SW) equations, the reference model for computational Hydraulics. The LBM has been successfully applied to multi-layered SW flows too (La Rocca et al., 2012, Prestininzi et al., 2013).

The simplicity of the standard LBM stems from the fact that the velocity space discretization is based on a low number of lattice velocities. On the other hand this simplicity implies a fundamental and serious drawback: transcritical and supercritical SW flows, which practically always occur in real-world hydraulic flows, cannot be simulated. Among such realistic flows, it is worth mentioning the propagation of a water front over dry bed, which physically implies the transition through critical state just upstream the propagation front.

However, if the number of lattice velocities is increased arbitrarily, i.e. tends to infinity, the representation of the exact Maxwellian equilibrium distribution function becomes better and better and the simulation of transcritical and supercritical SW flows becomes possible. This is the basic idea of the Gas Kinetic Method (hereinafter GKM), developed by Prendergast and Xu (1993) and Xu and Prendergast (1994) and later applied successfully to the simulation of SW flows on structured (Ghidaoui et al., 2001) and unstructured (Liang et al., 2007) grids. In particular, the ability of the GKM in simulating different transcritical flows on wet bottoms is shown in Liang et al. (2007).

The capability of handling wet/dry fronts is crucial to the development of any SW model aimed at providing technically grounded results. One of the most crucial problems in numerically handling wet/dry

fronts is the unstable behavior shown by many algorithms in the wet/dry edge, very often characterized by the onset of physically meaningless negative water depths. The effect is severely aggravated by irregular topographies, which is usually the case in practical applications.

The most common approaches are: (i) the ones derived from Brufau et al. (2002), who adopted a temporary modification of the bed elevation that renders the cell completely wet; (ii) the ones derived from Bradford and Sanders (2002) and Begnudelli and Sanders (2006), who substitute the momentum equation at front interface with an extrapolation of the particle velocity from the wet portion to the dry one; (iii) the ones derived from Tao (1984), who introduces a porous bed in order to avoid the distinction between wet and dry elements. Similar approaches have been adopted by several authors in the field of Boussinesq-type equations for run-up problems in Coastal Hydraulics (Ip et al., 1998; Kennedy et al., 2000) and more recently for complex SW flows over irregular terrains (Hou et al., 2013).

The capability of handling wet-dry fronts within the framework of GKM has been preliminary assessed in Prestininzi et al. (2014), where the authors apply a consolidated numerical algorithm (Ghidaoui et al., 2001 Liang et al., 2007) to the numerical simulation of the propagation of wet-dry fronts, adopting a non-Minimum Positive Depth (hereinafter non-MPD). In Prestininzi et al. (2014) this approach, based on an *ad hoc* formulation of the inter-cell fluxes of the wet-dry front cells, was applied mainly to the propagation of wet-dry fronts on frictionless bottom. In this work we want to extend the assessment of the GKM performed in Prestininzi et al. (2014) to the simulation of SW flows propagating over rough, dry bottom, carrying out comparisons with several experimental benchmark cases.

The structure of the paper is as follows: firstly, a brief presentation of the GKM; secondly, the description of the treatment of the wet-dry interface; thirdly, the description of the benchmark cases considered; fourthly, the presentation and the discussion of the results.

2 THE GAS KINETIC METHOD AND THE SHALLOW WATER EQUATIONS

Consider the Probability Distribution Function (hereinafter PDF) $f=f(x,y,c_x,c_y,t)$, which gives the probability of finding a fluid particle at time t, at point $\mathbf{P}$ ($\mathbf{P} \equiv \mathbf{i}x+\mathbf{j}y$), with velocity $\mathbf{c}$ ($\mathbf{c}\equiv\mathbf{i}c_x+\mathbf{j}c_y$). x, y are the horizontal spatial coordinates, whose unit vectors are $\mathbf{i}$, $\mathbf{j}$ respectively. The time evolution of the PDF is governed by the Boltzmann equation:

$$\frac{\partial f}{\partial t} + c_x \frac{\partial f}{\partial x} + c_y \frac{\partial f}{\partial y} + F_x \frac{\partial f}{\partial c_x} + F_y \frac{\partial f}{\partial c_y} = \frac{f^e - f}{\tau} \tag{1}$$

where F_x, F_y are the horizontal components of the external force vector per unit mass. According to equation (1) the PDF is advected by the particle velocity $\mathbf{c}$ (which does not coincide with the flow velocity) and affected by external forces by fourth and fifth term at LHS. The term at RHS is the collision term, which represents the modification of the PDF due to the interactions (collisions) with other particles. The collision term is represented by means of the collision operator at RHS of (1), which is linear with respect to the PDF f (Bhatnagar-Gross-Krook, 1954). The Bhatnagar-Gross-Krook collision operator expresses the relaxation of the PDF function f towards the local Maxwellian equilibrium f^e in a time τ. Consider the following expression for the equilibrium PDF (Ghidaoui et al., 2001; Deng et al.; 2001):

$$f^e = \frac{1}{\pi g} e^{-\frac{(\mathbf{c}-\mathbf{u})\cdot(\mathbf{c}-\mathbf{u})}{gh}} \tag{2}$$

where $\mathbf{u}$ ($\mathbf{u}\equiv\mathbf{i}u+\mathbf{j}v$) is the flow velocity vector, whose Cartesian components are u, v along x and y axis respectively. h is the flow depth and g is the gravity acceleration. Equation (1) together with the definition (2) for the equilibrium PDF is equivalent to the SW equations. For the sake of simplicity the equivalence is not shown here. Details can be found in Prestininzi et al. (2014). It is enough to say that the equivalence is based on the following properties, which hold exactly for vanishing τ.

$$\begin{cases} hu = \int_{-\infty}^{+\infty}\int_{-\infty}^{+\infty} c_x f dc_x dc_y,\ hv = \int_{-\infty}^{+\infty}\int_{-\infty}^{+\infty} c_y f dc_x dc_y \\ hu^2 + g\frac{h^2}{2} = \int_{-\infty}^{+\infty}\int_{-\infty}^{+\infty} c_x^2 f dc_x dc_y\,, huv = \int_{-\infty}^{+\infty}\int_{-\infty}^{+\infty} c_x c_y f dc_x dc_y, hv^2 + g\frac{h^2}{2} = \int_{-\infty}^{+\infty}\int_{-\infty}^{+\infty} c_y^2 f dc_x dc_y \end{cases} \tag{3}$$

In other words, for vanishing τ, the first and second statistical moment of the equilibrium PDF with respect to the particle velocity $\mathbf{c}$ coincide with the conservative terms of the Shallow Water equations:

$$\begin{cases} \frac{\partial h}{\partial t}+\frac{\partial hu}{\partial x}+\frac{\partial hv}{\partial y}=0 \\ \frac{\partial hu}{\partial t}+\frac{\partial}{\partial x}\left(hu^2+g\frac{h^2}{2}\right)+\frac{\partial}{\partial y}(huv)=-F_x \\ \frac{\partial hu}{\partial t}+\frac{\partial}{\partial x}(huv)+\frac{\partial}{\partial y}\left(hv^2+g\frac{h^2}{2}\right)=-F_y \end{cases} \quad (4)$$

the latter can then formally expressed by:

$$\begin{cases} \frac{\partial h}{\partial t}+\frac{\partial}{\partial x}\left(\int_{-\infty}^{+\infty}\int_{-\infty}^{+\infty}c_x f dc_x dc_y\right)+\frac{\partial}{\partial y}\left(\int_{-\infty}^{+\infty}\int_{-\infty}^{+\infty}c_y f dc_x dc_y\right)=0 \\ \frac{\partial hu}{\partial t}+\frac{\partial}{\partial x}\left(\int_{-\infty}^{+\infty}\int_{-\infty}^{+\infty}c_x^2 f dc_x dc_y\right)+\frac{\partial}{\partial y}\left(\int_{-\infty}^{+\infty}\int_{-\infty}^{+\infty}c_x c_y f dc_x dc_y\right)=-F_x \\ \frac{\partial hu}{\partial t}+\frac{\partial}{\partial x}\left(\int_{-\infty}^{+\infty}\int_{-\infty}^{+\infty}c_x c_y f dc_x dc_y\right)+\frac{\partial}{\partial y}\left(\int_{-\infty}^{+\infty}\int_{-\infty}^{+\infty}c_y^2 f dc_x dc_y\right)=-F_y \end{cases} \quad (5)$$

External force components F_x, F_y are given by:

$$F_x=gh\left(\frac{\partial z_f}{\partial x}+n_m^2 u\frac{\sqrt{\mathbf{u}\cdot\mathbf{u}}}{h^{4/3}}\right), F_y=gh\left(\frac{\partial z_f}{\partial y}+n_m^2 v\frac{\sqrt{\mathbf{u}\cdot\mathbf{u}}}{h^{4/3}}\right) \quad (6)$$

being z_f ($z_f \equiv z_f(x, y)$) the bottom topography and n_m the Manning roughness coefficient. The basis for the GKM formulation of the SW equations is represented by equations (5): practically they are equivalent to a LBM formulation with an infinite number of particle velocities. According to Liang et al. (2007), equation (1) can be solved analytically neglecting fourth and fifth term at LHS. The result is:

$$f=f|_{t=t_0}e^{-\frac{t-t_0}{\tau}}+\frac{1}{\tau}\int_{t_0}^{t}e^{-\frac{t-\theta}{\tau}}f^e d\theta \quad (7)$$

Substituting (7) in equations (5), the GKM formulation of the SW equations is finally obtained. Integrals at RHS of (5) can be calculated in terms of the PDF f at time t_0, the flow velocity **u** and the flow depth h.

3 TREATMENT OF THE WET-DRY INTERFACE

In this work the finite-volume approximation of equations (5) of Ghidaoui et al. (2001), Liang et al. (2007) is considered on a structured mesh defined on the *xy* plane (Prestininzi et al., 2014).

In order to define the numerical algorithm, it is necessary to calculate the integral at right hand side of (5), adopting the expression (7) for the PDF. The technique is explained in Ghidaoui et al. (2001) and Liang et al., (2007) and applied in Prestininzi et al. (2014). Due to its cumbersome aspects, this is not reported here for the sake of simplicity. The reader is directly referred to these works for details.

Treatment of wet-dry fronts deserves particular attention. Indeed realistic Shallow Water flows very often imply the presence of such fronts, which is a major source of numerical instability. The latter stems from the fact that some calculations require the computation of primitive variables (velocity components u and v) in a framework which uses the conservative variables hu and hv. The division by some numerically small h always introduces high rounding errors possibly leading to instabilities.

In this work the wet-dry fronts are treated according to a slightly modified non-MPD approach (Prestininzi et al., 2014), which assures a correct handling of the wetting phase by setting a minimum threshold for the depth. Differently from purely non-MPD approaches, this minimum value is not initially set over the whole domain which, in this case, is actually dry. When the depth in a computational volume grows above zero but lower than the threshold, the numerical fluxes are all substituted by their analytical formulation in the limit for abitrary small h: $h \rightarrow 0$.

Such a treatment avoids overflow. The resulting scheme recovers the analytical transition over dry bed obtainable by considering the eigenstructure of the Riemann problem (Toro, 2001) and is here found to be extremely robust, allowing for very low values of the threshold to be used. No particular treatment is adopted for the drying phase. The depth is just set to zero when falling below the threshold. In order to fulfill the mass balance when employing high threshold values, such subtracted volume is distributed among the wet surrounding cells, proportionally to the previously calculated depth.

4 RESULTS

In order to validate the finite volume formulation of the GKM in simulating SW flows with both transcritical regimes and wet-dry interface on rough bottom, several benchmark cases are taken into consideration.

The first benchmark case is the 1D steady motion over a given frictionless bottom profile. Although this flow does not have any wet-dry front and occurs on a frictionless bottom, nevertheless it is considered in order to show the correctness of the implementation of the numerical algorithm.

The second benchmark case is the 1D dam-break problem on a rough dry bottom, experimentally realized by Lauger and Hager (1998).

The third benchmark case is selected from the CADAM (Concerted Action on DAm-Break Modeling) project (Morris, 2000), which provides useful benchmarks for numerical verification of dam-break flow propagation.

Finally, the fourth and last benchmark case is the 2D dam break in a 90° bend, realized experimentally by Soares-Frazão and Zech (2002).

4.1 *1D steady motion over a smooth bottom profile*

The 1D steady flow over a smooth bottom profile is considered in a 1D channel discretized by means of 800 square cells. The bottom profile is described by the Gaussian function:

$$z_f = z_{MAX} e^{-\frac{(x-x_0)^2}{\sigma^2}} \tag{8}$$

The exact solution can be easily obtained in terms of flow depth h by means of the Bernoulli's theorem:

$$h + z_f + \frac{q^2}{2gh^2} = const \tag{9}$$

The flow velocity u is obtained by means of: $u=q/h$, being q the discharge per unit width of the channel, constant with respect to x. Results are plotted in Fig. 1, where analytical and GKM numerical flow depth (Fig. 1a), flow velocity and Froude number (Fig. 1b) are shown. Abscissa x, flow depth h and flow velocity u are scaled with respect to the half-length of the channel $L/2$, h_u and $\sqrt{gh_u}$ respectively, being h_u the upstream flow depth.

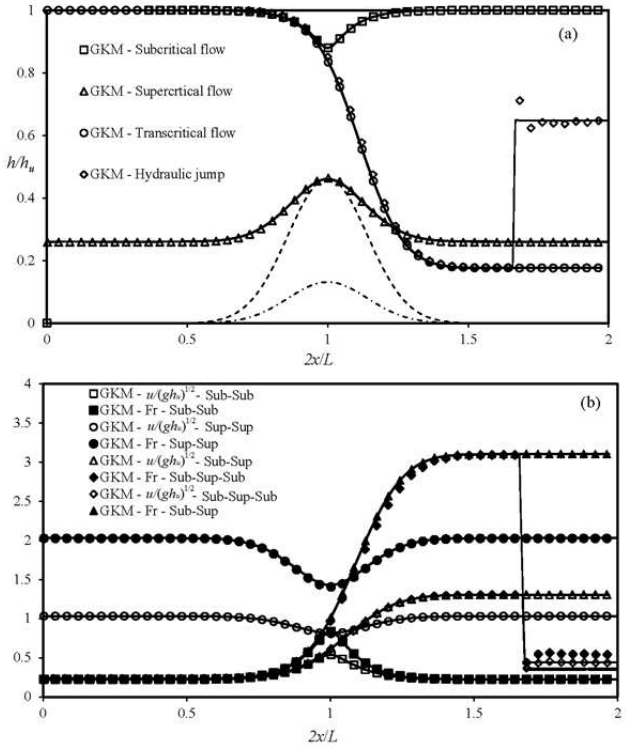

Figure 1. Steady motion over a smooth bottom profile. a) Flow depth profiles. b) Dimensionless velocity and Froude number profiles. Suffix "Sub" stands for Subcritical regime, suffix "Sup" for Supercritical regime. Continuous traces are analytical solution from equation (9).

In Fig. 1a (upper panel) the dashed line is the bottom profile of the supercritical flow, while the dot-dashed line is the bottom profile of both the sub- and transcritical flow. The overall qualitative agreement is very good. From a quantitative point of view, the approximation error has been estimated as:

$$E(p) = \frac{1}{N}\sqrt{\sum_{i=1,N}\left(\frac{p_{GKM,i}-p_{Ref,i}}{p_{Ref,i}}\right)^2} \tag{11}$$

where the generic quantity p is considered both numerically (p_{GKM}) and analytically or experimentally (the reference value p_{Ref}). This error has been calculated for the flow depth h and the x-velocity component u and has been found in the range: $3\times10^{-5} < E(h), E(u) < 5\times10^{-3}$ for all of the cases considered in Fig. 1. The position of the GKM numerical hydraulic jump agrees quite well with the position of the hydraulic jump, determined analytically for the Subcritical-Supercritical-Subcritical case. The oscillations near the shock are due to the second order nature of the proposed GKM.

4.2 *1D dam-break on a dry, rough bottom*

To demonstrate the applicability of the proposed GKM to 1D dam break flows over dry, rough bed, the experimental dam-break flow results of Lauber and Hager (1998) are considered for testing shock-capturing capability in dry, rough beds. The experimental set-up used by Lauber and Hager (1998) consists of a reservoir with a gate placed at x_0= 3.315m in a channel, 14.0m long. The initial water depth h_I is equal to 0.3 m. The roughness of the channel is characterized by a Manning roughness coefficient n_m equal to $0.01 m^{-1/3}s$.

In Fig. 2 the flow depth (upper panel) and velocity (lower panel) profiles are shown at different instants of times. All the quantities in Fig. 2 are dimensionless: flow depth is scaled with respect to h_I, flow velocity to $(gh_I)^{1/2}$, the length of the channel to h_I and the time to $h_I/(gh_I)^{1/2}$. The considered instants in the upper panel are: 0.97, 1.94, 2.91, 3.89, 4.86, 5.83, 6.80. The considered instants in the lower panel are: 0.97, 1.94, 3.89, 7.77, 9.72.

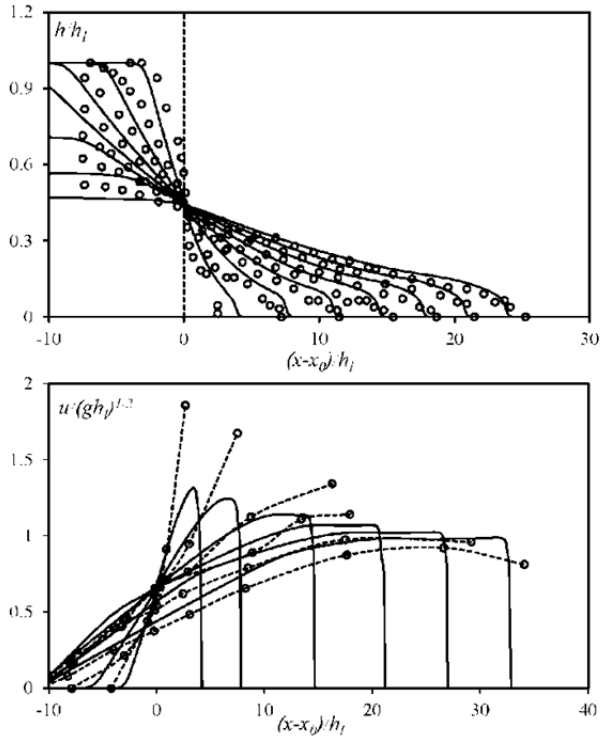

Figure 2. Dimensionless flow depth (upper panel) and velocity (lower panel) profiles along the channel at $t/h_I/(g\ h_I)^{1/2}$=0.97, 1.94, 2.91, 3.89, 4.86, 5.83, 6.80 (upper panel) and at $t/h_I/(g\ h_I)^{1/2}$=0.97, 1.94, 3.89, 7.77, 9.72 (lower panel). Solid line: GKM numerical results.

The agreement between GKM numerical results and the experimental results of Lauber and Hager (1998) is satisfactory. It is interesting to observe (upper panel of Fig. 2) that the propagation characteristics of the front as well as its shape, affected by the bottom roughness, are correctly reproduced by numerical results. The error (11) has been calculated for the flow depth h. Its order of magnitude has been found in the range $10^{-2}\div10^{-1}$ for all of the cases considered in Fig. 2.

4.3 *The CADAM test case*

The experimental set-up (Morris, 2000) consists of a reservoir, 15.5m long, closed by a gate and followed by a rectangular channel, 38m long. The initial flow depth in the reservoir is 0.75m. Moreover, a symmetric triangular bump, 0.4m high, 6m long, is placed at x_B=13m downstream of the gate. The roughness of the channel is characterized assuming a Manning coefficient equal to 0.0125m$^{-1/3}$s. Several gauge stations are placed at different positions. Numerical simulations have been carried out considering the bottom completely dry.

In Fig. 4, experimental and GKM numerical flow depth time histories at x=19.5m (left panel) and x=28.5m (right panel) are shown. Experimental time histories are relative to gauge station G4 and G13, located 4m and 13m downstream of the gate respectively (Morris, 2000). In Fig. 4 numerical results are represented by dots, while the solid lines represent experimental data.

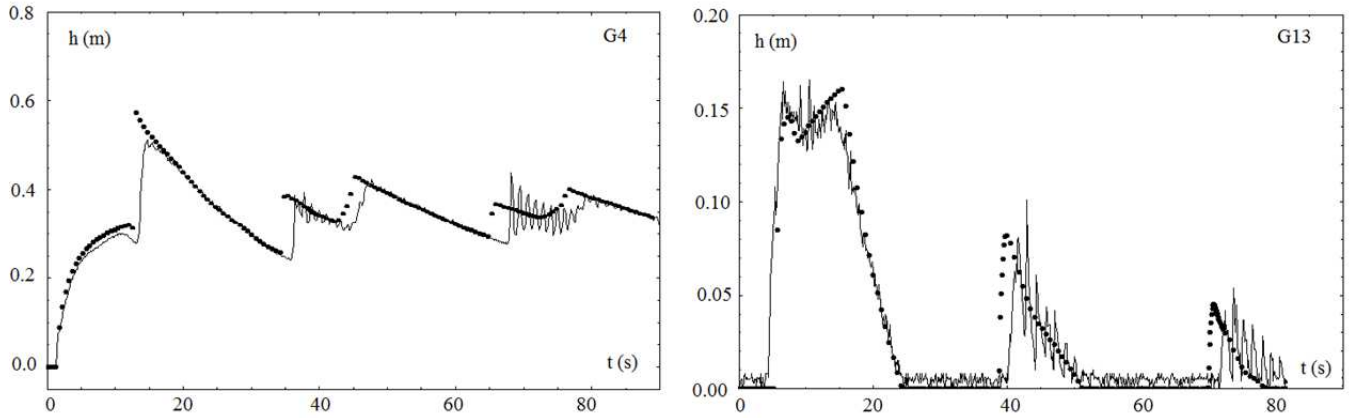

Figure 4. Experimental and GKM numerical flow depth time histories. Left panel: results relative to gauge station G4. Right panel: results relative to gauge station G13. Dots: GKM numerical results. Solid line: experimental results.

Also in this case the agreement is quite satisfactory and the error (11), calculated for the flow depth h, had an order of magnitude in the range $10^{-2}\div10^{-1}$.

In Fig. 5, two snapshots of the GKM numerical flow depth and Froude number profiles along the channel are shown at t=1.8s and t=4.2s. Solid lines represent the flow depth profiles and dashed lines the Froude number profiles. Dots represent the initial flow depth profile (before the dam-break). At t=1.8s the flow has not reached the bump yet, while at t=4.2s, the flow has reached and overcome the bump. It is interesting to observe the transitions occurring at t=4.2s: a continuous sub-supercritical transition downstream of the bump, a discontinuous super-subcritical transition (a hydraulic jump) just at the basis of the bump and finally a continuous sub-supercritical transition at the top of the bump.

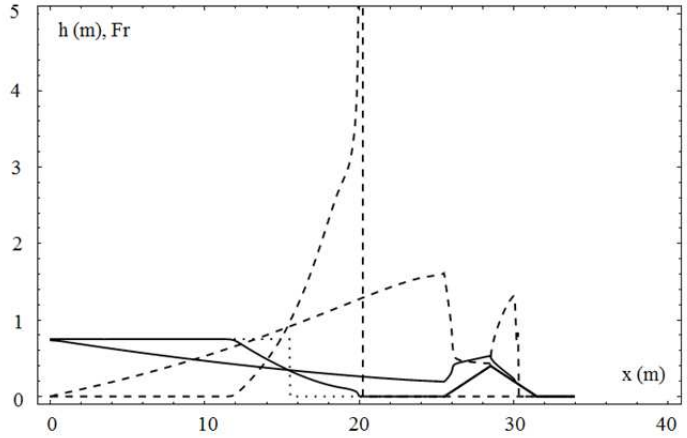

Figure 5. Snapshots of the GKM numerical flow depth and Froude number profiles along the channel at t=1.8s and t=4.2s. Solid lines: flow depth profiles. Dashed lines: Froude number profiles. Dots: initial flow depth profile.

4.4 *2D dam break in a 90° bend*

The setup consists of an upstream square reservoir connected to a rectangular channel with a 90° degree bend (Soares-Frazão and Zech (2002). The Manning coefficient n_m is assumed equal to 0.006m$^{-1/3}$s. Gauges are used to measure the flow depth time histories at different locations.

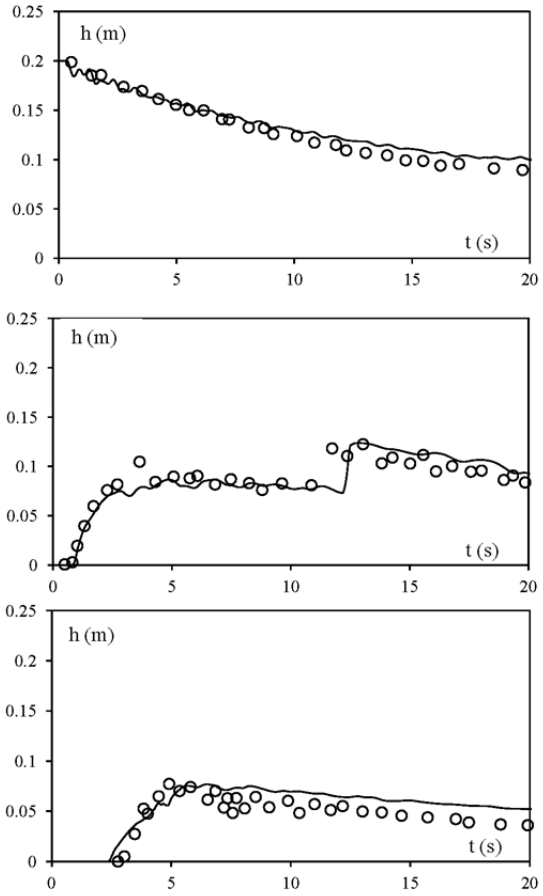

Figure 6. Flow depth time histories obtained from probes 1 (upper panel) and 3 (lower panel). Solid lines: GKM numerical results. Dots experimental results of Soares-Frazão and Zech (2002).

In this work flow depth time histories obtained from probes 1, 3 and 5 (Soares-Frazão and Zech (2002) are considered and used for comparison with GKM numerical results (Fig. 6). Gauge 1 is located within the reservoir. Gauge 3 is located within the channel, upstream of the bend, at x=1.85m from the reservoir. Gauge 5 is located within the channel, downstream of the bend, at y=1.5m from the bend. In Fig. 6 the solid lines represent GKM numerical results, while dots represent experimental results of Soares-Frazão and Zech (2002). Upper panel is relative to probe 1, middle panel to probe 3, lower panel to probe 5. The agreement is fairly satisfactory, although differences between numerical and experimental data are evident in Fig. 6, as time goes by, probably due to the fact that source terms modeling is not balanced in the proposed model.

5 CONCLUSIONS

This work is aimed at assessing of the ability of the GKM in dealing with 1D and 2D SW flows and it can be seen as the prosecution of a previous work, where the same GKM finite-volume numerical formulation was presented and applied to simulate fundamental benchmark cases of both 1D and 2D SW flows.

Here the authors focused particularly on the role of the roughness in 1D dam-break flow and on the ability in simulating a rather complex 2D flow, such as the 2D dam-break in a 90° bending channel.

Results can be considered fairly good for 1D SW flows, being the effect of roughness well interpreted by the GKM. With respect to the 2D SW flow considered in this work, results are satisfactory. Improvements are expected by a balanced modeling of the source terms. Considerable work is currently being carried out along these lines.

NOTATION

x	horizontal spatial coordinate
y	horizontal spatial coordinate
t	time
f	probability density function

f^e	equilibrium probability density function
τ	relaxation time
c_x	fluid particle velocity - x component
c_y	fluid particle velocity - y component
g	gravity acceleration
F_x	external force - x component
F_y	external force - y component
h	flow depth
u	x-flow velocity component
v	y-flow velocity component
$\mathbf{u}$	flow velocity vector
n_m	Manning's roughness coefficient
z_f	bottom topography
t_0	reference time
θ	dummy variable
z_{MAX}	peak of the Gaussian bottom
x_0	position of the peak in the Gaussian bottom, position of the dam
σ	variance of the Gaussian bottom
q	discharge per unit width
h_u	upstream flow depth
h_l	flow depth at the left of the dam
$p_{GKM,i}$	i^{th} numerical data of the generic quantity p
$p_{Ref,i}$	i^{th} reference data of the generic quantity p
N	number of considered data

REFERENCES

Aidun, K., Clausen, J.R. (2010). Lattice-Boltzmann Method for Complex Flows. Annual Review of Fluid Mechanics. Vol. 42, pp. 439–472.

Begnudelli, L., Sanders, B.F. (2006). Unstructured grid finite volume algorithm for shallow-water flow and scalar transport with wetting and drying. J. of Hydraulic Eng., ASCE, Vol. 132, No. 4, pp. 371–384.

Bhatnagar, P.L., Gross, E.P., Krook, M. (1954). A Model for Collision Processes in Gases. I. Small Amplitude Processes in Charged and Neutral One-Component Systems. Phys. Rev. Vol. 94, pp. 511-525.

Bradford, S.F., Sanders, B.F. (2002). Finite-volume model for shallow water flooding of arbitrary topography. J. of Hydraulic Eng., ASCE, Vol. 128, No. 3, pp. 289 –298.

Brufau, P., Vàzquez-Cendòn, M.E., Garcìa-Navarro, P. (2002). A numerical model for the flooding and drying of irregular domains. International Journal For Numerical Methods In Fluids, Vol. 39, pp. 247–275.

Deng, J.Q., Ghidaoui, M.S., Gray, W.G., Xu, K. (2001). A Boltzmann-based mesoscopic model for contaminant transport in flow systems. Advances in Water Resources. Vol. 24, pp. 531-550.

Ghidaoui, M.S., Deng, J.Q., Gray, W.G., Xu, K. (2001). A Boltzmann based model for open channel flows. Int. J. Numer. Meth. Fluids. Vol. 35. pp. 449–494.

Hou, J., Liang, Q., Simons, F., Hinkelmann, R., (2013). A stable 2D unstructured shallow flow model for simulations of wetting and drying over rough terrains. Computers and Fluids, Vol. 82, pp. 132-147.

Ip, J.T.C., Lynch, D.R., Friedrichs, C.T., (1998). Simulation of estuarine flooding and dewatering with application to Great Bay, New Hampshire. Estuarine, Coastal and Shelf Science, Vol. 47, pp. 119–141.

Kennedy, A.B., Chen, Q., Kirby, J.T., Dalrymple, R.A., (2000). Boussinesq modelling of wave transformation, breaking and runup. I: one dimension. Journal of Waterway, Port, Coastal and Ocean Engineering, Vol. 126, pp. 39–47.

La Rocca, M., Adduce, C., Lombardi, V., Sciortino, G., Hinkelmann, R. (2012). Development of a lattice Boltzmann method for two-layered shallow-water flow. International Journal for Numerical Methods in Fluids. Vol. 70, No. 8, pp. 1048-1072.

Lauber, G., Hager, W.H., (1998). Experiments to dam-break wave: horizontal channel. J. Hydraul. Res. Vol. 36, No. 3, pp. 291–307.

Liang, J.H., Ghidaoui, M.S., Deng, J.Q., Gray, W.G. (2007). A Boltzmann-based finite volume algorithm for surface water flows on cells of arbitrary shapes. Journal of Hydraulic Research. Vol. 45. pp. 147–164.

Morris, M., (2000). CADAM: Concerted Action on Dam-break Modeling – Final Report. Rep. SR 571. HR Wallingford.

Prendergast, K.H., Xu, K. (1993). Numerical Hydrodynamics from Gas-Kinetic Theory. Journal of Computational Physics. Vol. 109, pp. 53-66.

Prestininzi P, Sciortino G, La Rocca M. (2013). On the effect of the intrinsic viscosity in a two-layer shallow water lattice Boltzmann model of axisymmetric density currents. Journal of Hydraulic Research. Vol. 51, No. 6, pp 668-680.

Soares Frazão, S., Zech, Y., (2002). Dam break in channels with 90° bend. J. Hydraul. Eng., ASCE. Vol. 128. No. 11, pp. 956–968

Succi, S. (2001).The Lattice Boltzmann Equation for Fluid Dynamics and Beyond. Clarendon press. Oxford.

Toro, E.F., (2001). Shock-capturing methods for free-surface shallow/flows, Wiley, New York.

Xu, K., Prendergast, K.H. (1994). Numerical Navier-Stokes Solutions from Gas-Kinetic Theory. Journal of Computational Physics. Vol. 114, pp. 9-17.

Zhou, J. (2004). Lattice Boltzmann Methods for Shallow Water Flows. Springer, New York.